Injury, Int. J. Care Injured 50 (2019) 939–949

Contents lists available at ScienceDirect

Injury

journal homepage: www.elsevier.com/locate/injury

Clustering of morphological fracture lines for identifying intertrochanteric fracture classification with Hausdorff distance–based K-means approach

Jiantao Li[a,1], Shaojie Tang[b,1], Hao Zhang[a,1], Zhirui Li[a], Wanyu Deng[c], Chen Zhao[c], Lianghui Fan[c], Guoqi Wang[d], Jianheng Liu[a], Peng Yin[e], Gaoxiang Xu[a], Licheng Zhang[a,*], Peifu Tang[a,*]

[a] Department of Orthopaedics, Chinese PLA General Hospital, No. 28 Fuxing Road, Beijing, 100853, China
[b] School of Automation, Xi'an University of Posts and Telecommunications, Xi'an, Shanxi, 710121, China
[c] School of Computer, Xi'an University of Posts and Telecommunications, Xi'an, Shanxi, 710121, China
[d] Department of Pediatrics, Chinese PLA General Hospital, No. 28 Fuxing Road, Beijing 100853, China
[e] Department of Orthopedics, Beijing Chaoyang Hospital, Capital Medical University, No. 8 Gong Ren Ti Yu Chang Nan Lu Rd, Beijing 100020, China

ARTICLE INFO

Article history:
Accepted 17 March 2019

Keywords:
Intertrochanteric fracture classification
3D-CT
Orphological fracture lines
Hausdorff distance
K-means

ABSTRACT

Objectives: The aim of this study was to develop a systematic three-dimensional (3D) classification of intertrochanteric fractures by clustering the morphological features of fracture lines using the Hausdorff distance–based K-means approach and assess the usefulness of it in the clinical setting.
Methods: We retrospectively analyzed the data of 504 patients with intertrochanteric fractures who underwent closed reduction and intramedullary internal fixation. The morphological fracture lines of all patients extracted from computed tomography were transcribed freehand onto the template. All fracture lines were then clustered into five distinct types using the Hausdorff distance–based K-means clustering method. Five radiographic parameters and four functional parameters were used to evaluate the postoperative functional states and mobilization levels. Postoperative complications were also recorded.
Results: Intertrochanteric fractures were classified into five types: type I (108/504, 21.4%), simple fracture with intact lateral femoral wall and greater trochanter fragment; type II (85/504, 16.9%), simple fracture with intact lateral femoral wall with/without lesser trochanter detachment; type III (147/504, 29.2%), fractures with intertrochanteric crest detachment involving the lesser trochanter and greater trochanter with an intact lateral femoral wall; type IV (113/504, 22.4%), fractures with large intertrochanteric crest detachment and large lesser trochanter and greater trochanter detachment partially involving the lateral femoral wall and less medial cortical support; type V (51/504, 10.1%), a combination of pertrochanteric and lateral fracture line involving the entire lateral femoral wall and lesser trochanter detachment. Parameters of femoral neck–shaft angle and sliding distance of the cephalic nail were significantly different among types. The complication rate generally increased from type I to type V ($P = 0.035$).
Conclusions: The unsupervised clustering can achieve identification of the type of intertrochanteric fractures with clinical significance. The Tang classification can be used to describe fracture morphology, predict the possibility of achieving stable reduction and the risk of complications following intramedullary fixation.

Introduction

Several intertrochanteric fracture classification systems have been proposed and used in clinical practice for decades, including the Evans [1], Jensen [2], Boyd-Griffin [3], Kyle [4], and AO/OTA classifications [5]. However, these "classic" X-ray–based classification systems are thought to be insufficient and have limited ability to provide detailed explanations and accurate information about the actual fracture morphology,

* Corresponding authors at: Chinese PLA General Hospital, No. 28 Fuxing Road, Beijing 100853, China.
E-mail addresses: zhanglcheng218@126.com (L. Zhang), pftang301@163.com (P. Tang).
[1] The first three authors contributed equally to this work.

https://doi.org/10.1016/j.injury.2019.03.032
0020-1383/

especially those involving large oblique fragments that include the lesser trochanter [6–10]. With advances in radiography, computed tomography (CT) and three-dimensional (3D)-CT have been widely used in clinical settings to provide precise evaluation and diagnosis in orthopedics. A method for the fracture stratification of differences in 3D intertrochanteric fracture patterns is required to explain the morphology and fracture mechanism.

Recent studies have re-evaluated intertrochanteric fracture classifications and introduced new criteria based on CT data [10–12]. However, most of these classification systems are not reliable and are inadequate for postoperative prediction. Moreover, few reports have examined the relationship between the morphological features of the fracture lines and clinical outcomes.

Here we collected 504 intertrochanteric fractures of preoperative CT data and focused on a clustering analysis of morphological fracture lines to identify classifications. Based on the classifications, the radiographic parameters, postoperative functions, and complications were collected and compared. The purpose of this study was to classify the intertrochanteric fractures of 3D models based on the unsupervised clustering method and assess the usefulness of this new classification in the clinical setting.

Materials and methods

Between September 2009 and March 2017, 963 patients with intertrochanteric hip fractures treated with intramedullary device. Inclusion criteria were as follows: (1) CT data of the proximal femur obtained before surgical intervention; (2) CT images with a thickness < 3.0 mm; (3) a minimum of 1 year of radiographic follow-up; (4) age ≥ 18 years; and (5) low-energy mechanism of injury. We excluded patients according to the following: (1) pathological fractures; (2) mental disorders; (3) walking with assistive devices before the fractures; (4) fractures with associated neurovascular injuries; and (5) previous surgery or osteoarthritis on the affected hip joints. According to the inclusion and exclusion criteria, 504 patients were included in this study.

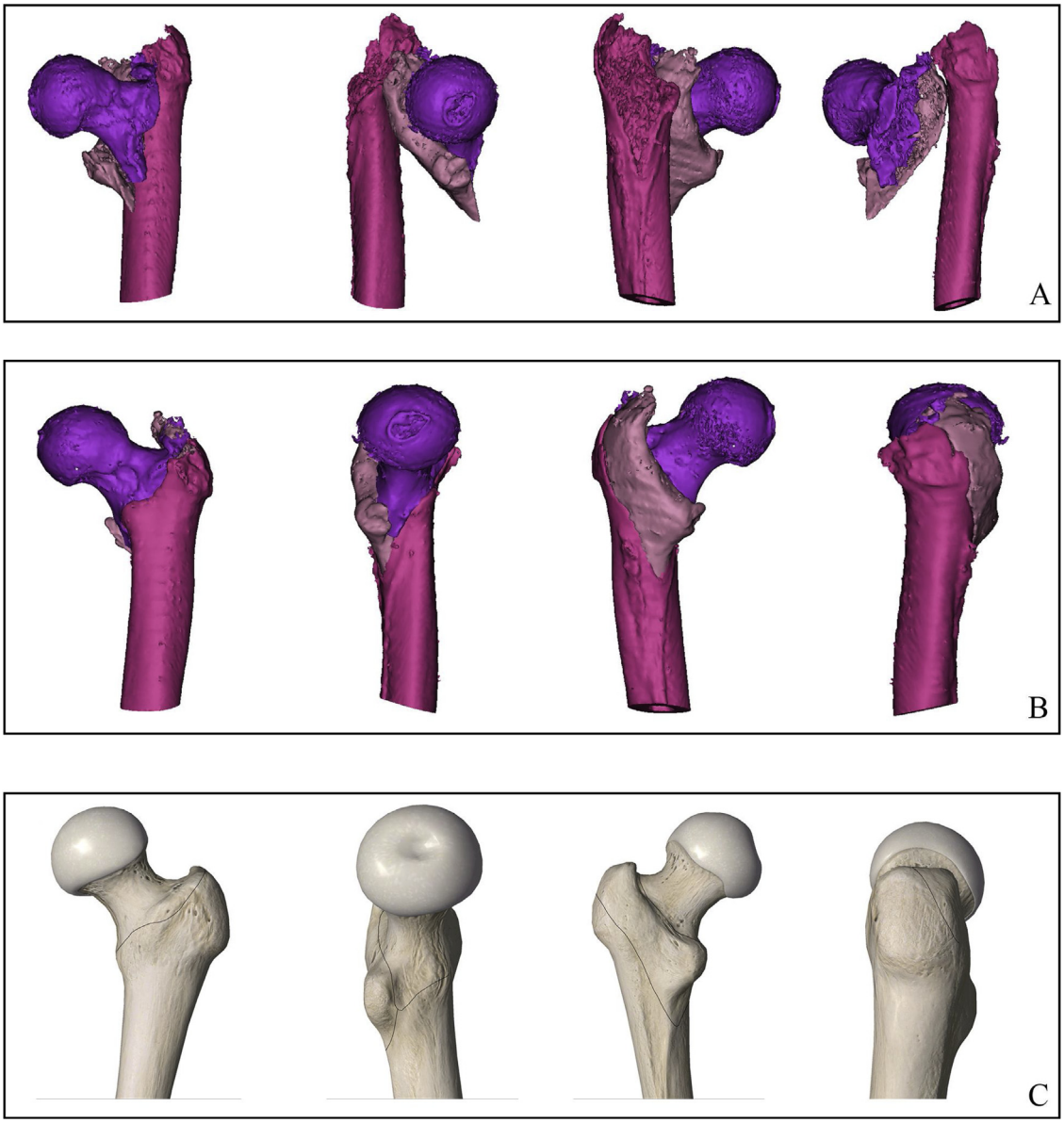

Fig. 1. Images illustrating the fracture line method. (A) Every fragment was reconstructed in Mimics. (B) Fracture fragments were selected for reduction in the 3D view. (C) Fracture lines were transcribed freehand onto the two-dimensional template in Adobe Photoshop.

Description of morphological fracture lines

Proximal femoral templates

An Essential Skeleton 4 (3D4 Medical, San Diego, CA, USA) was used to export the typical anterior, posterior, medial, and lateral images of a 3D proximal femur that was positioned in the anatomic plane. The above four two-dimensional (2D) images were imported into Adobe Photoshop CC 2015 (Adobe Systems Software Ireland, Dublin, Ireland) as templates for the fracture mapping.

Fracture models

The original Digital Imaging and Communications in Medicine (DICOM) files of CT data were collected and imported into Mimics 15.0 (Materialise, Leuven, Belgium). We reconstructed all 3D fragments of each patient using the software. With application of the move and rotate function, each fragment was virtually reduced in the 3D view. Consequently, the fracture lines could be clearly observed. These reductive fracture models were then modified to develop 2D images that were presented in the same anatomic plane as the templates. With Mimics and Adobe Photoshop open side by side, the fracture lines were transcribed freehand onto the template layer (Fig. 1). Overlapping of the layers showed the fracture maps (Fig. 2).

Hausdorff distance–based K-means clustering of the morphological feature dataset

After exporting the four views, each view corresponding to a picture with fracture lines for each patient case, we exploited a Hausdorff distance–based K-means approach to automatically cluster the five fracture-line types from the 504 cases. The flow chart of the proposed clustering method for fracture-line types is shown in Fig. 3.

Preparation of input data

Suppose all cases are represented by $\{X_i|i = 1, \ldots, I\}$. In this work, we enrolled $I = 504$ cases. The preparation of a case with original fracture lines involved four pictures: anterior, medial, posterior, and lateral views. We programmed and implemented an algorithm to combine these four pictures together into a larger image to simultaneously consider their effects on the clustering later. In this way, one case was corresponding to one image to standardize the fracture lines for each case (Fig. 4).

Hausdorff distance

Euclidean distance cannot be directly adopted to demonstrate the differences among cases since the total number of pixels on the fracture lines differ. Hausdorff distance is a good choice to overcome this difficulty. Thus, we assume the following:

$$H_{mn} = H(X_m, X_n) = \max[h(X_m, X_n), h(X_n, X_m)],$$

$$h(X_m, X_n) = \max_{xm} \min_{xn} \|x_m - x_n\|, \; x_m \in X_m, \; x_n \in X_n,$$

where the pixels x_m and x_n are on the cases X_m and X_n, respectively.

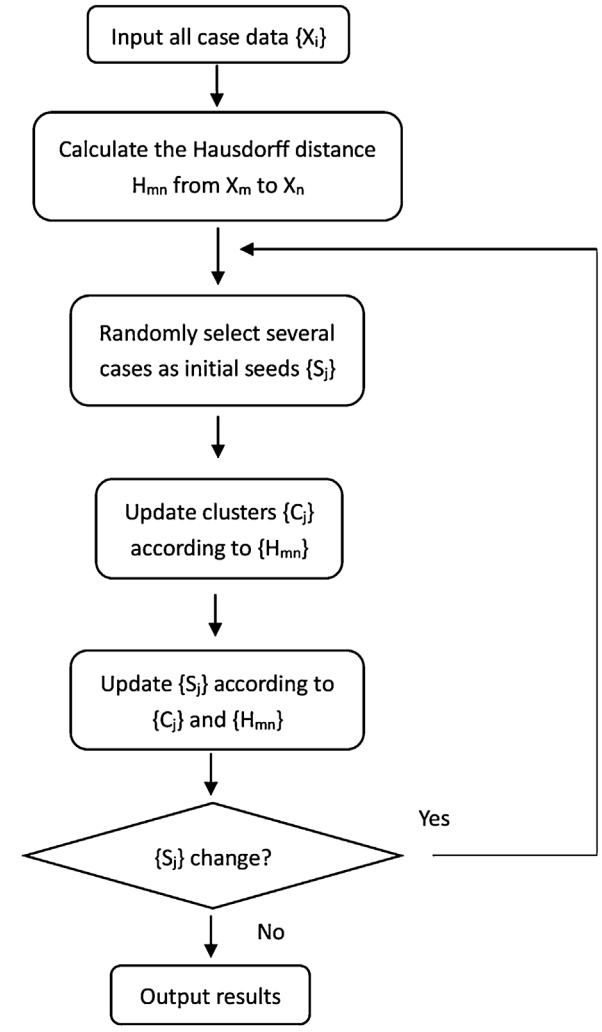

Fig. 3. Flow chart of the proposed clustering method for fracture-line subtypes.

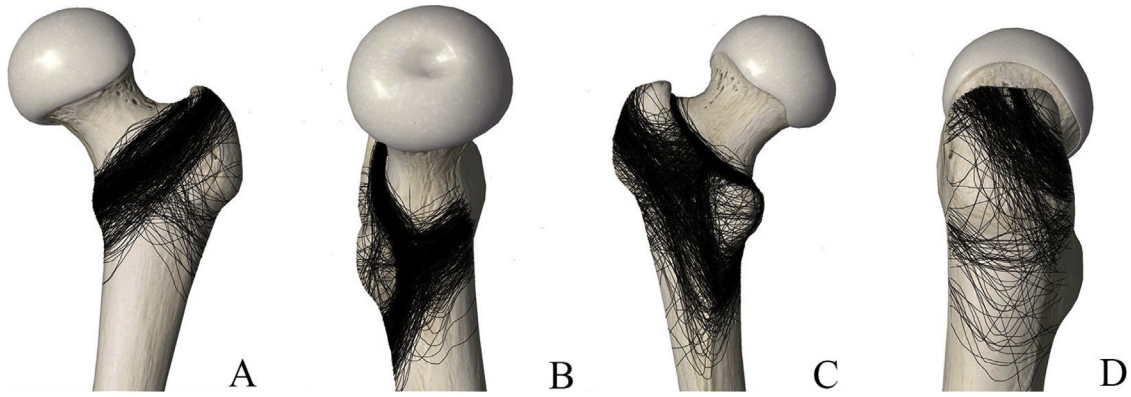

Fig. 2. Overlapping of all layers showing the fracture maps in four orthogonal views: (A) anterior, (B) medial, (C) posterior, and (D) lateral.

Fig. 4. We extracted the fracture lines from each case (A) and then programmed and implemented an algorithm (B), connecting each line on the different views together to make a fracture line model (C) to simultaneously consider their effects on the clustering analysis.

Random selection of initial seeds

Several cases are randomly selected as initial seeds for the K-means approach since it is performed iteratively. That is, all seeds are represented by $\{Sj|j = 1, \ldots, J\} \subset \{X_i\}$. The concrete number of the selected seeds are determined empirically by the physician. In this study, the number is fixed as J = 5. According to the principle of the K-means approach, the final result after convergence is independent of the selection of the initial seeds although a local optimal solution may be acquired. To escape from a local optimal, initial seeds shall be randomly selected several times under the physician's judgement of whether a reasonable result has been achieved.

K-means clustering

The K-means approach is effective for clustering for various practical applications. The K-means clustering considers each case as a point in the feature space and classifies all I data points into K disjoint clusters. The core of the K-means clustering method is to iteratively update {Sj} according to $\{H_{mn}\}$. One round of iteration involves two steps as described below:

(i) Taking case X_m as an example, we need to first judge which of the clusters $\{Cj|j = 1, \ldots, J\}$ it belongs to as follows:

$X_m \in C_{j(k)} \subset \{X_i\}$, if $H_{mk} = \min\{H_{mn}|X_n = S_{j(n)}, j(n) = 1, \ldots, J\}$,

where

$Sj \in Cj$,

$C_{j1} \cap C_{j2} = \emptyset$, if $j_1 \neq j_2$, and

$C_1 \cap C_2 \cap \ldots \cap CJ = \{X_i\}$; and

(ii) After the clusters have been determined for all cases, we then update {Sj} according to $\{H_{mn}\}$,

For all $X_m \in Cj$, we calculate

$\Theta_m = \Sigma_n(H_{mn}|X_n \in C_j)$,

and if $X_k \in Cj$ is the minimum in $\{\Theta_m\}$, then we have the update of seed $Sj = X_k$.

For all clusters {Cj}, we repeat the above operation, thereby updating their corresponding seeds {Sj}.

Stopping criterion

The stopping criterion we adopted for the iteration procedure of the above-mentioned K-means clustering is the first time as {Sj} is not changed. According to the principle of K-means approach, there will be definitely no update after this point of time.

Clinical evaluations

This study was approved by the Ethics Committee of the Chinese PLA General Hospital and was registered at isrctn.com (ISRCTN30974801).

All patients were treated with the indirect reduction and percutaneous surgical techniques and participated in similar rehabilitation protocols. Postoperative radiography was used to assess the reduction condition and hardware related complication. Time from fracture to surgery, duration of the surgical procedure, and intraoperative bleeding volume were recorded. The duration of surgery was noted in concordance with the anesthesiology records. We used the following methods to evaluate the surgical outcomes.

Radiography parameters

Parameters were measured on the radiographs obtained immediately postoperative and the final follow-up using the

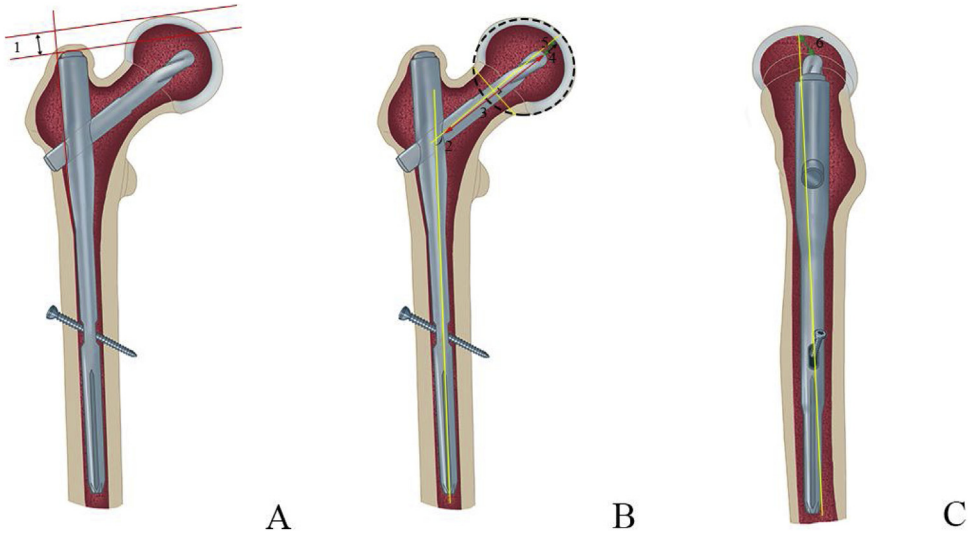

Fig. 5. (A) This measurement was done by drawing line 1, the distance designated as the femoral head height (FHH); (B) angle 2 was formed by the femoral shaft line and the axis of the femoral neck; line 3 was the distance between the tip of the cephalic nail and the medial edge of the shaft nail; line 4 was the distance from the tip of cephalic nail to the femoral head cortex, which was co-linear with line 3; line 5 was from the tip of the lag screw to the apex of the femoral head. (C) Line 6 was from the tip of the lag screw to the apex of the femoral head on the lateral radiograph.

measuring devices on the digital screen. All of the results were calibrated according to the ratio of the known diameter of the cephalic nail to its diameter on the digital image.

Femoral head height

The femoral head height (FHH; Fig. 5, line 1) relative to the nail was calculated to evaluate the reduction loss. This measurement was done by drawing two lines perpendicular to the shaft nail: one placed at the superior edge of the nail and one placed at the top of femoral head. The FHH was defined as the distance between these two lines.

Femoral neck shaft angle

Femoral neck shaft angle (FNSA; Fig. 5, angle 2) was measured as the angle formed by the femoral shaft and the femoral neck shaft.

Medial cephalic nail length (L_{mcn})

L_{mcn} (Fig. 5, line 3) was the line from the cephalic nail tip to the medial edge of proximal shaft nail. The difference of L_{mcn} in two periods indicated the sliding distance.

Tip–cortex distance

Tip–cortex distance (TCD; Fig. 5, line 4), co-linear with line 3, was the distance between the cephalic nail tip and the femoral head cortex.

Tip–apex distance

The tip–apex distance (TAD) was proposed by Baumgaertner et al. [13] using X-ray radiographs to evaluate nail position (Fig. 5, sum of lines 5 and 6).

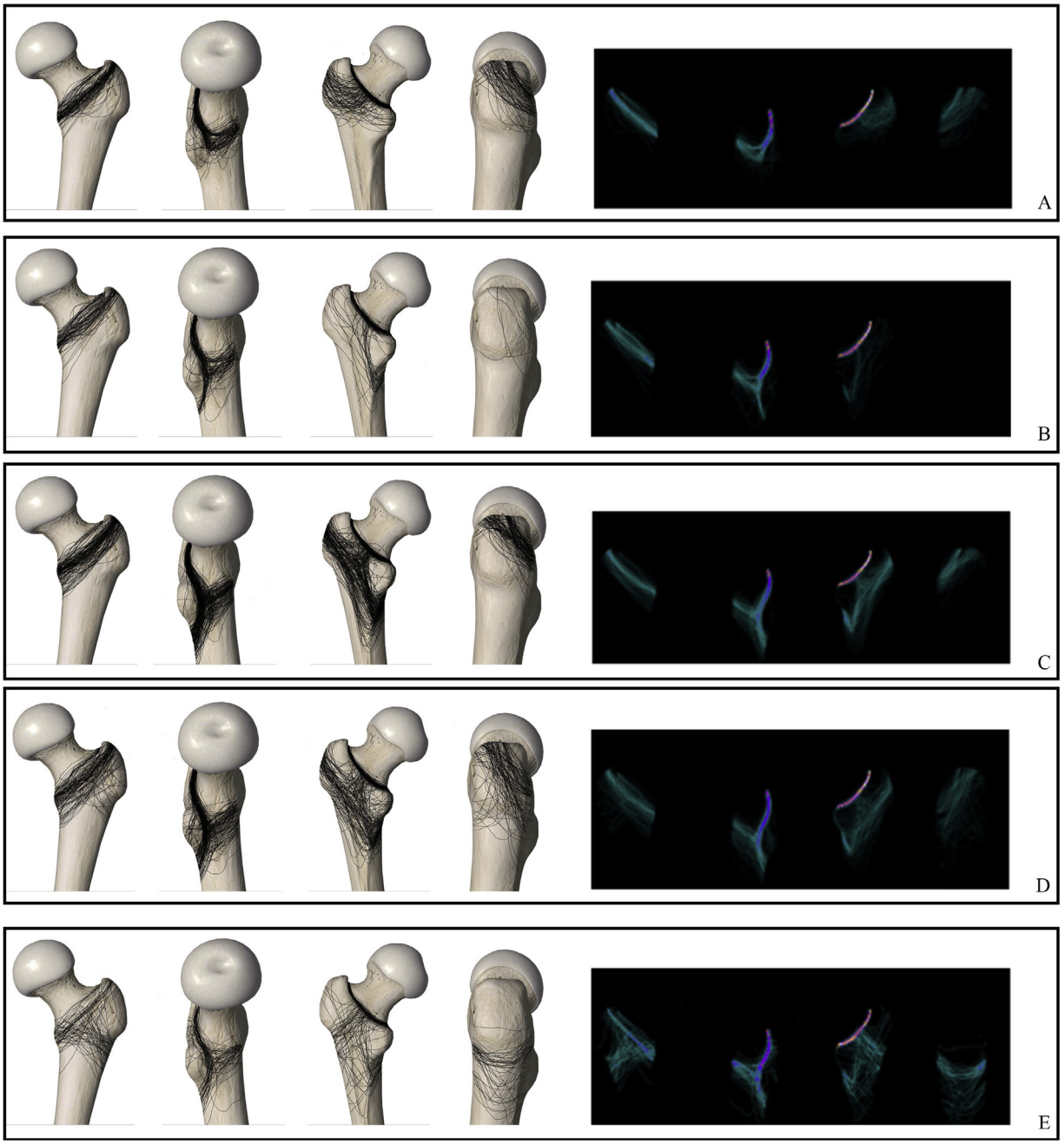

Fig. 6. The clustering results and pseudocolor maps of the five fracture types, which exhibit intergroup differences and intergroup consistency.

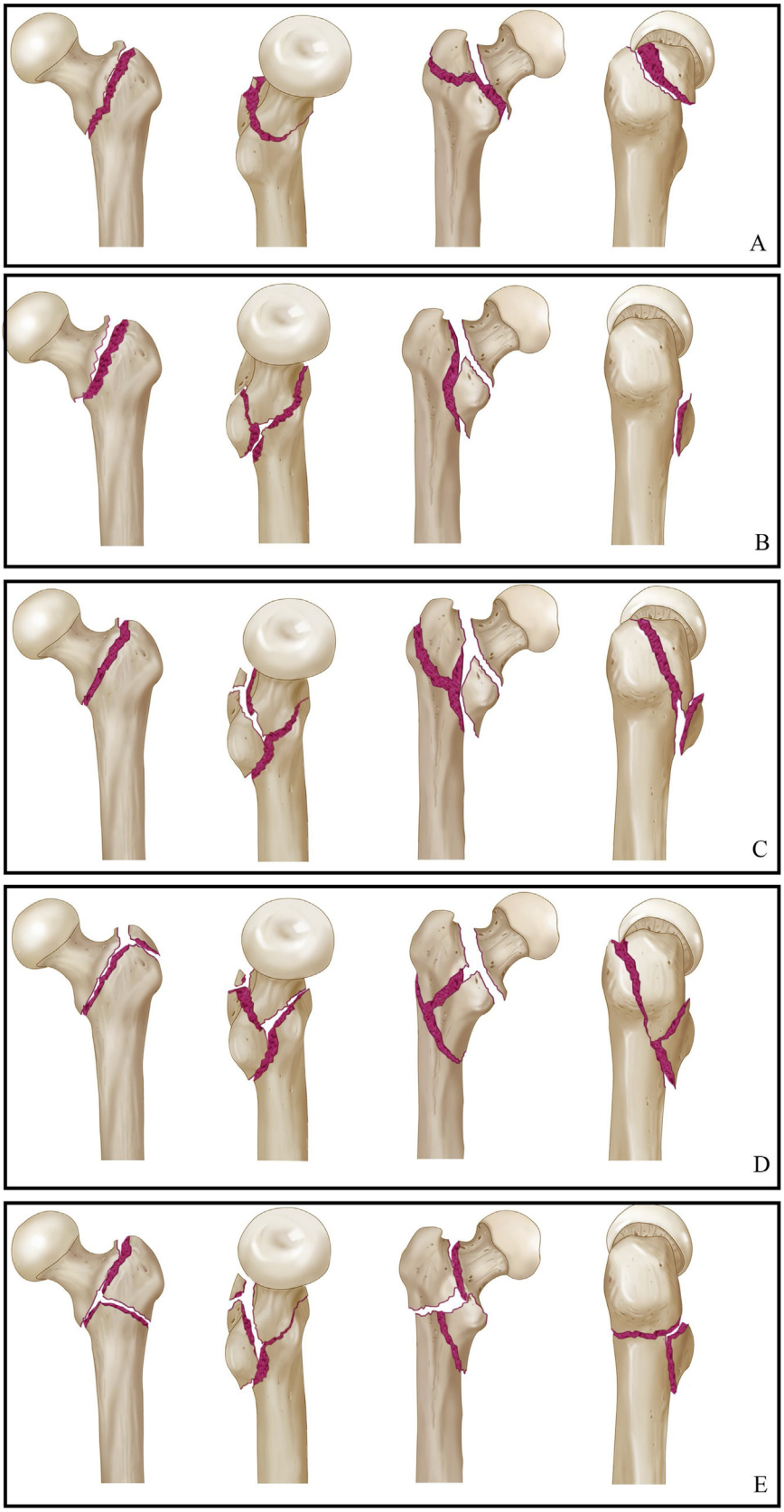

Fig. 7. Type I, simple fracture with intact lateral femoral wall and greater trochanter fragment.
Type II, simple fracture with intact lateral femoral wall with lesser trochanter detachment or not.
Type III, fractures with intertrochanteric crest detachment involving the distal lesser and proximal greater trochanter and an intact lateral femoral wall.
Type IV, fractures with large intertrochanteric crest detachment with large distal lesser and proximal greater trochanter detachment partially involving the lateral femoral wall with less medial cortical support.
Type V, a combination of pertrochanteric and lateral fracture line involving the entire lateral femoral wall and lesser trochanter detachment.

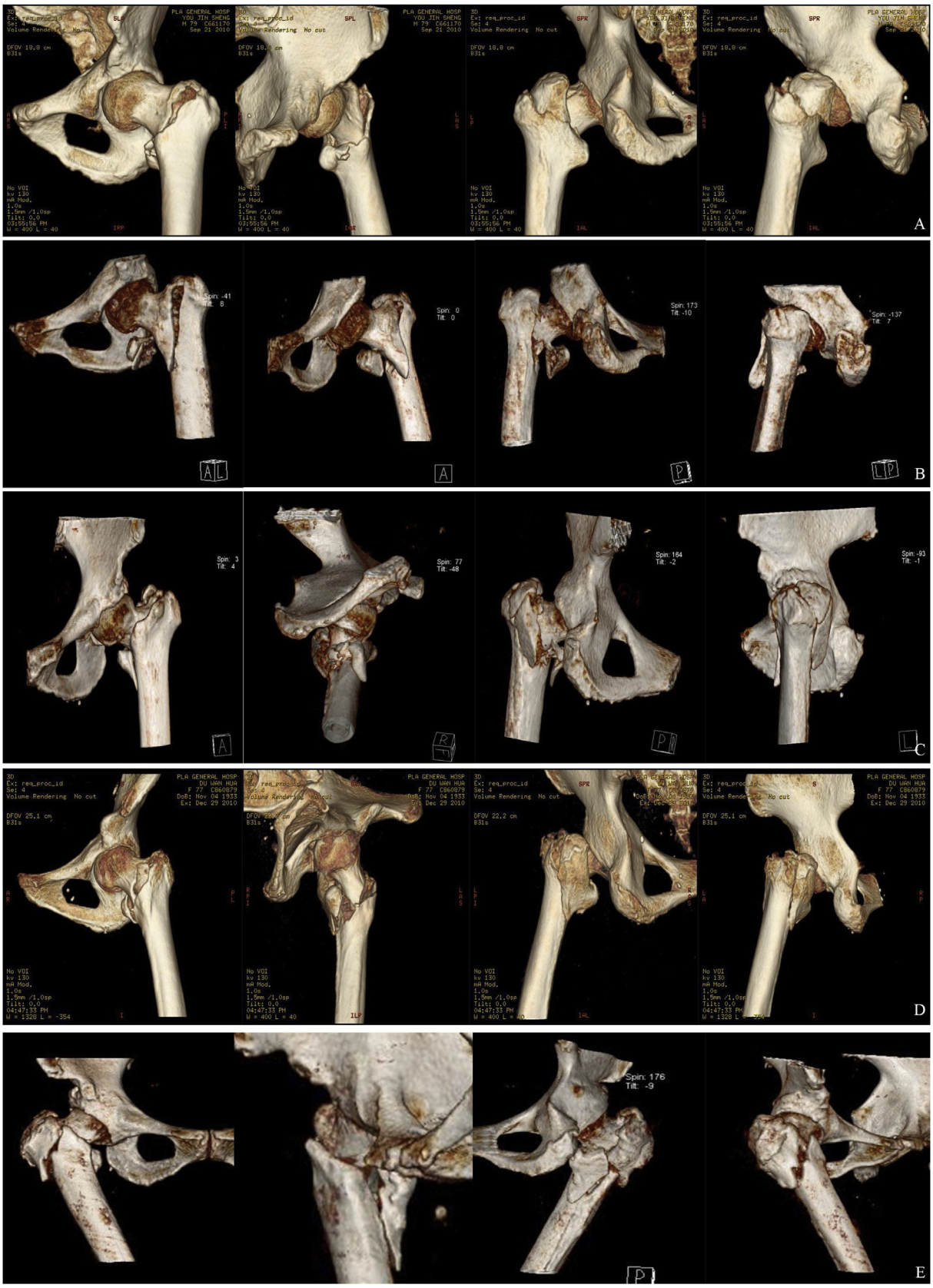

Fig. 8. The 3D-CT of the intertrochanteric fractures. (A) Type I; (B) type II; (C) type III; (D) type IV; (E) type V.

Functional parameters

At the final follow-up, the functional outcome was evaluated by the Functional Independence Measure (FIM) [14], Timed Up and Go (TUG) test (the time taken to rise from a sitting position, walk 3 m at a comfortable pace, turn, walk back to the chair, and sit back down) [15,16], 2-minute walk test (2MWT) [17], and Parker-Palmer scores [18], which were used to assess the physical function.

Complications

Reduction loss, implant breakage, excessive sliding, nonunion, cut-out, infection, periprosthetic fracture, and loss of mobility were the complications that were recorded. We defined reduction loss as a change of FNSA > 10°. We defined excessive sliding as a sliding distance ≥ 10 mm.

Statistical analysis

The SPSS (version 19.0; SPSS Inc., Chicago, IL, USA) was used to evaluate the data. We used the chi-square and Fisher's exact tests to analyze the categorical variables among the types. One-way analysis of variance was used to compare the continuous variables among types and the Tukey's multiple comparison was used to test post hoc. P values <0.05 were considered as statistical significance.

Results

Patient characteristics

The mean age was 80.21 ± 12.95 years old (range, 20–103 years). The mean height was 163.13 ± 8.19 cm (range, 140–185 years). The mean weight was 70.00 ± 12.67 kg (range, 35–100 kg). The 195 male and 309 female patients had 252 right and 252 left hip fractures. The mean period of follow-up was 16 months (range, 12–23 months).

Five 3D intertrochanteric fracture classifications

With the proposed clustering analysis, all 504 morphological intertrochanteric fracture maps were classified into five types. We exported the pseudocolor map to exhibit the intertype difference and intratype consistency on which we proposed the classification system (Fig. 6).

The five types included: type I (108/504, 21.4%), type II (85/504, 16.9%), type III (147/804, 29.2%), type IV (113/504, 22.4%), and type V (51/504, 10.1%) (Figs. 7 and 8).

Radiography parameters

The distribution of patient characteristics in the classification is shown in Table 1. Intraoperative bleeding volumes were higher in patients with type V than in those with other types ($p < 0.001$). Changes in FNSA and sliding distance of the cephalic nail were statistically different ($p < 0.001$) (Fig. 9A, B).

Functional parameters

The number of patients for whom FIM parameters and Parker-Palmer scores were determined is shown in Table 2. The FIM scores by type are shown in Fig. 9C.

The proportion of patients able to complete the TUG and 2MWT is shown in Table 3. The distances achieved on the 2MWT by type are shown in Fig. 9D.

Complications

Sixty patients experienced fracture-related complications; of them, 39 underwent reoperation (five with type I, five with type II, 10 with type III, 14 with type IV, and five with type V). The risk of requiring a reoperation was 4.6% in type I, 5.9% in type II, 6.8% in type III, 12.4% in type IV, and 9.8% in type V (Table 4).

Discussion

In this present study, we reconstructed the 3D models of 504 intertrochanteric fractures using preoperative CT data and utilized an unsupervised clustering analysis method of morphological fracture lines to identify 3D model classification. The system classified the fractures into five types according to involvement of the medial cortices or lateral femoral wall. And the characteristics of fracture line indicated that the size of the intertrochanteric crest detachment affected the fragments of the greater and lesser trochanters. Based on the classifications, the clinical parameters, radiographic parameters, postoperative function, and complications were collected and compared. This study showed that this new 3D model classification system concerning fragment size of the intertrochanteric crest, medial cortical support and lateral

Table 1
Patient demographics, inpatient details, and radiographic parameters by classification.

Description	Classification						
		Type I	Type II	Type III	Type IV	Type V	P value
Total number		108	85	147	113	51	
Sex	Female	75	48	94	61	31	0.144
	Male	33	37	53	52	20	
Side	Left	54	40	74	53	31	0.540
	Right	54	45	73	60	20	
Age (y)		81.23 ± 11.80	80.39 ± 13.59	81.11 ± 10.44	80.75 ± 13.71	73.98 ± 17.16	0.009*
Weight (kg)		58.47 ± 12.10	61.48 ± 13.34	61.05 ± 11.92	61.82 ± 12.87	63.68 ± 13.90	0.132
Height (cm)		161.63 ± 7.35	163.61 ± 8.90	162.86 ± 8.03	164.74 ± 8.12	162.75 ± 8.83	0.072
Body mass index		22.35 ± 4.00	22.84 ± 4.14	22.92 ± 3.74	22.70 ± 4.27	23.92 ± 4.54	0.267
Time from fracture to surgery (d)		7.49 ± 4.81	6.68 ± 3.92	7.75 ± 4.17	7.18 ± 4.49	8.57 ± 4.70	0.138
Surgery time (min)		96.80 ± 34.15	99.58 ± 35.42	96.83 ± 39.68	104.03 ± 54.97	114.16 ± 45.09	0.093
Intraoperative bleeding volume (mL)		119.54 ± 97.68	122.35 ± 88.64	125.00 ± 89.95	142.32 ± 128.72	197.16 ± 144.92	<0.001*
TAD (mm)		17.53 ± 6.93	20.78 ± 11.10	18.98 ± 7.72	19.79 ± 9.38	19.52 ± 8.30	0.112
Change of FHH (mm)		−3.47 ± 2.40	−3.33 ± 3.60	−3.68 ± 3.20	−4.10 ± 3.66	−4.33 ± 3.09	0.260
Change of FNSA (°)		−2.69 ± 2.58	−2.58 ± 2.32	−3.17 ± 3.44	−3.92 ± 2.69	−4.38 ± 2.72	<0.001*
Sliding distance of cephalic nail (mm)		2.31 ± 2.09	2.21 ± 1.89	2.50 ± 2.21	3.32 ± 2.53	3.78 ± 2.77	<0.001*
Change of TCD (mm)		−0.66 ± 1.67	−0.57 ± 1.24	−0.70 ± 1.71	−0.73 ± 0.86	−0.87 ± 1.37	0.823

TAD, tip–apex distance; FHH, femoral head height; FNSA, femoral neck–shaft angle.

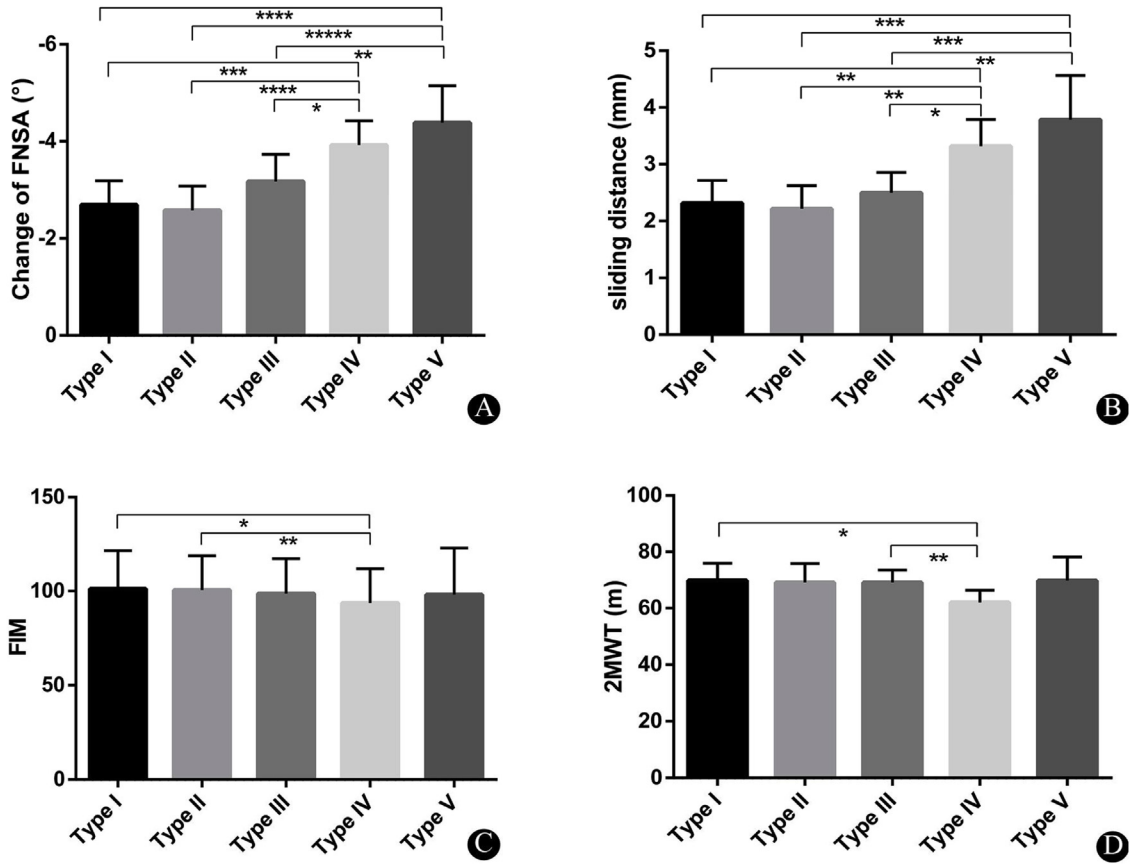

Fig. 9. (A) Change in femoral neck–shaft angle (FNSA) by type (*p = 0.036, **p = 0.009, ***p = 0.002, ****p = 0.001, *****p < 0.001). (B) Sliding distance by type (*p = 0.004, **p = 0.001, ***p < 0.001). (C) Functional Independence Measure (FIM) scores by type (*p = 0.008, **p = 0.021). (D) Two-minute walk test (2MWT) results by type (*p = 0.042, **p = 0.047).

Table 2
Functional ability by classification.

		Functional Independence Measure		Parker-Palmer score	
Classification	Numbers that got the parameters, n (%)	Mean (SD)	95% confidence interval	Mean (SD)	95% confidence interval
Type I (n = 108)	94 (87.0%)	101.19 (20.34)	97.03, 105.36	6.73 (2.22)	6.28, 7.19
Type II (n = 85)	75 (88.2%)	100.61 (18.21)	96.42, 104.80	7.17 (2.14)	6.68, 7.67
Type III (n = 147)	129 (87.8%)	98.72 (18.64)	95.47, 101.97	6.90 (1.87)	6.57, 7.23
Type IV (n = 113)	98 (86.7%)	93.63 (18.34)	89.96, 97.31	6.65 (2.00)	6.25, 7.05
Type V (n = 51)	45 (88.2%)	98.02 (24.95)	90.53, 105.52	7.36 (2.10)	6.72, 7.99
P value	0.997	0.071		0.232	

Table 3
Performance-based functional ability by classification measured using the Timed Up and Go Test and 2-Minute Walk Test.

Classification	Timed Up and Go Test, sec			2-Minute Walk Test, m		
	Proportion who completed test, n (%)	Mean (SD)	95% confidence interval	Proportion who completed test, n (%)	Mean (SD)	95% confidence interval
Type I (n = 108)	88 (81.5%)	17.42 (10.16)	15.27, 19.57	87 (80.6%)	69.90 (28.53)	63.82, 75.98
Type II (n = 85)	70 (82.4%)	17.96 (9.77)	15.63, 20.29	69 (81.2%)	69.12 (28.00)	62.39, 75.84
Type III (n = 147)	124 (84.4%)	17.86 (7.88)	16.46, 19.26	121 (82.3%)	69.17 (24.24)	64.80, 73.53
Type IV (n = 113)	90 (79.6%)	19.63 (12.38)	17.04, 22.23	88 (77.9%)	60.07 (20.45)	57.73, 66.40
Type V (n = 51)	43 (84.3%)	18.49 (10.41)	15.28, 21.69	42 (82.4%)	69.81 (26.98)	61.40, 78.22
P value	0.884	0.632		0.920	0.212	

femoral wall involvement which were vital factors in the treatment of the intertrochanteric fractures but did not be considered in the existing classifications [19–21], could provide an accurate prediction of the risk of complications following intramedullary fixation.

The clustering analysis aims to classify data into categories according to their similarity. It has been widely used in the research field of pattern recognition and image processing [22]. Using the K-means approach, data can be clustered into groups

Table 4
Complications by classification.

Complication	Classification					
	Type I	Type II	Type III	Type IV	Type V	P value
Loss of reduction	0	0	1	2	2	0.035*
Excessive sliding of the cephalic nail	0	1	3	4	2	
Cut-out	1	1	2	2	1	
Implant breakage	1	1	1	2	1	
Nonunion	0	1	0	0	0	
Infection	1	0	2	1	0	
Periprosthetic fracture	1	0	2	3	0	
Loss of mobility	2	2	2	3	1	
Contralateral hip fracture	1	2	2	4	2	
Total (%)	7 (6.5%)	8 (9.4%)	15 (10.2%)	21 (18.6%)	9 (17.6%)	60 (11.9%)

characterized by the small distance to their corresponding centers. The fracture lines we extracted from any case are generally different from those extracted from others since the total number of pixels on the fracture lines for each case are likely very different. Hausdorff distance is inherently capable of tolerating fracture line complexity, whereas Euclidean distance is too rigid to be directly adopted for demonstrating the differences among cases; therefore, we chose Hausdorff distance as the basis on which the fracture line types are successfully clustered in this work. Meanwhile, we use the pseudocolor map to exhibit intertype difference and intratype consistency according to which we proposed the 3D classification system.

In the present study, all of the intertrochanteric fractures were classified into five types. According to the morphological feature and clinical evaluation, types I, II, and III were characterized by the intact femoral lateral wall and sufficient medial cortical support, making it easy to obtain direct cortical contact during surgery. These three types were considered the stable patterns, which required less surgical time, involved less intraoperative bleeding volume, had better functional recovery, and resulted in lower complication rates. Type IV and V fractures were suffered from the significantly sliding distance of the cephalic nail and changes in FNSA. Patients with type IV had poorer clinical function demonstrated by worse FIM and 2MWT results than the other types. While patients with type V did not correlate with functional impairment, it was possible that the mean age of patients with type V was significantly younger than those of the other types. The complications in types IV and V were relatively higher than those of other types. Type IV fractures featured less medial cortical support and partial involvement of the lateral femoral wall and tended to be iatrogenic lateral femoral wall fractures, which inverted the fracture type from IV to V and complicated the fractures. The medial cortices can provide medial support and avoid femoral head varus [23], and the intact lateral wall can provide lateral support that prevents lateral sliding of the proximal fragment and distal shaft medialization [24]. We consider types I, II, and III stable fractures and types IV and V unstable fractures. We named this fracture system the Tang classification.

The course of intertrochanteric fracture lines is associated with muscle insertions and ligament attachments to the proximal femur [25]. The bone structures lack muscles and ligaments (bone uncovered area) forming the locus minoris resistentiae for the occurrence and spread of fracture lines. The uncovered area in the proximal femur, which results from some variability in soft-tissue attachment size and location, leads to the variability of intertrochanteric fracture fragments. The uncovered area of the anterior view of the proximal femur is formed by the iliofemoral ligament, vastus lateralis, and vastus medialis. Most pertrochanteric fracture lines run preferably along this area. The lower edge of the vastus lateralis is where the area of the lateral fracture line occurs. The uncovered area of the medial side is within the insertions of the vastus medialis, pectineus, iliopsoas, and articular capsule. The course of the fracture line on the medial side can run along the edge of the articular capsule with the lesser trochanter intact or along the area between the upper edges of the vastus medialis and pectineus and the lower edge of the iliopsoas with lesser

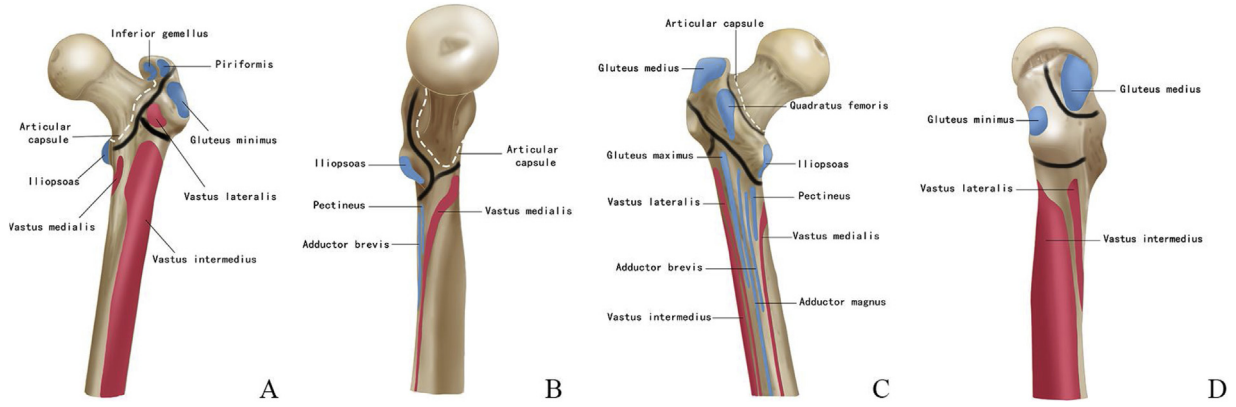

Fig. 10. (A) The uncovered area of the anterior view of the proximal femur is formed by the iliofemoral ligament, vastus lateralis, and vastus medialis. Most pertrochanteric fracture lines run preferably along this area (black line). The lower edge of the vastus lateralis is where the area of the lateral fracture line occurs (black line). (B) The course of the fracture line (black line) on the medial side can run along the edge of the articular capsule with the lesser trochanter intact or along the area between the upper edges of the vastus medialis and pectineus and the lower edge of the iliopsoas with lesser trochanter detachment. (C) The uncovered area of the posterior side is under the intertrochanteric crest. The uncovered area of the posterior basal part of the femoral neck is outside the attachment of the articular capsule, along which the course of the break line always runs (black line). (D) The uncovered area of the lateral view is within the edges of the gluteus medius and minimus, which form the great trochanter coronal fragment.

trochanter detachment. The uncovered area of the posterior side is under the intertrochanteric crest. The quadrate tubercle on the intertrochanteric crest is attached by the quadratus femoris, which may affect the multiple fragment size of the intertrochanteric crest. The uncovered area of the posterior basal part of the femoral neck is outside the attachment of the articular capsule, along which the course of the break line always runs. The uncovered area of the lateral view is within the edges of the gluteus medius and minimus, which form the great trochanter coronal fragment (Fig. 10).

This study has several limitations. First, we performed a subjective simplification by drawing fracture lines using the major fracture fragments. Second, our study is retrospective in nature and all operations were performed by five senior orthopedic surgeons who likely have individual surgical technique preferences. More prospective randomized controlled trials are needed to verify the usefulness of this new classification system. However, to the best of our knowledge, this is the first report of 3D intertrochanteric classification that uses the unsupervised clustering analysis. Moreover, our database was relatively large compared to those of previous studies.

Conclusion

The unsupervised clustering method used in this study can achieve type identification of intertrochanteric fractures with clinical significance. The Tang classification proposed here can be used to describe the morphologic fracture information, improve preoperative planning, and predict the possibility of obtaining stable reduction and the risk of complications following intramedullary fixation.

Conflicts of interest

There are no conflicts of interest of all authors.

Funding statement

This work was supported by the capital health research and development of special grants (2016-1-5012).

References

[1] Evans EM. The treatment of trochanteric fractures of the femur. J Bone Joint Surg Br 1949;31b(May 2)190–203 Epub 1949/05/01.
[2] Jensen JS. Classification of trochanteric fractures. Acta Orthop Scand 1980;51 (October 5)803–10 Epub 1980/10/01.
[3] Boyd HB, Griffin LL. Classification and treatment of trochanteric fractures. Arch Surg (Chicago, Ill: 1920) 1949;58(June 6)853–66 Epub 1949/06/01.
[4] Kyle RF, Gustilo RB, Premer RF. Analysis of six hundred and twenty-two intertrochanteric hip fractures. J Bone Joint Surg Am 1979;61(March 2)216–21 Epub 1979/03/01.
[5] Marsh JL, Slongo TF, Agel J, Broderick JS, Creevey W, DeCoster TA, et al. Fracture and dislocation classification compendium – 2007: Orthopaedic Trauma Association classification, database and outcomes committee. J Orthop Trauma 2007;21(November-Dececember Suppl. 10)S1–S133 Epub 2008/03/07.
[6] Cavaignac E, Lecoq M, Ponsot A, Moine A, Bonnevialle N, Mansat P, et al. CT scan does not improve the reproducibility of trochanteric fracture classification: a prospective observational study of 53 cases. Orthop Traumatol Surg Res 2013;99(February 1)46–51 Epub 2012/12/29.
[7] Shen J, Hu F, Zhang L, Tang P, Bi Z. Preoperative classification assessment reliability and influence on the length of intertrochanteric fracture operations. Int Orthop 2013;37(April 4)681–7 Epub 2012/12/21.
[8] Cho JW, Kent WT, Yoon YC, Kim Y, Kim H, Jha A, et al. Fracture morphology of AO/OTA 31-a trochanteric fractures: a 3D CT study with an emphasis on coronal fragments. Injury 2017;48(February 2)277–84 Epub 2017/01/04.
[9] Isida R, Bariatinsky V, Kern G, Dereudre G, Demondion X, Chantelot C. Prospective study of the reproducibility of X-rays and CT scans for assessing trochanteric fracture comminution in the elderly: a series of 110 cases. Eur J Orthop Surg Traumatol 2015;25(October 7)1165–70 Epub 2015/07/05.
[10] Shoda E, Kitada S, Sasaki Y, Hirase H, Niikura T, Lee SY, et al. Proposal of new classification of femoral trochanteric fracture by three-dimensional computed tomography and relationship to usual plain X-ray classification. J Orthop Surg 2017;25(January 1) 2309499017692700. Epub 2017/02/18.
[11] Futamura K, Baba T, Homma Y, Mogami A, Kanda A, Obayashi O, et al. New classification focusing on the relationship between the attachment of the iliofemoral ligament and the course of the fracture line for intertrochanteric fractures. Injury 2016;47(8):1685–91.
[12] T N. Proximal femoral fracture: seikeigeka (orthopaedics). 2014 842-50 p.
[13] Baumgaertner MR, Curtin SL, Lindskog DM, Keggi JM. The value of the tip-apex distance in predicting failure of fixation of peritrochanteric fractures of the hip. J Bone Joint Surg Am 1995;77(July 7)1058–64 Epub 1995/07/01.
[14] Granger CV. The emerging science of functional assessment: our tool for outcomes analysis. Arch Phys Med Rehabil 1998;79(March 3)235–40 Epub 1998/04/02.
[15] Sanders D, Bryant D, Tieszer C, Lawendy A, MacLeod M, Papp S, et al. A multicenter randomized control trial comparing a novel intramedullary device (InterTAN) versus conventional treatment (sliding hip screw) of geriatric hip fractures. J Orthop Trauma 2017;31(1):1–8.
[16] Morris S, Morris ME, Iansek R. Reliability of measurements obtained with the timed "up & go" test in people with Parkinson disease. Phys Ther 2001;81 (February 2)810–8 Epub 2001/02/15.
[17] Butland RJ, Pang J, Gross ER, Woodcock AA, Geddes DM. Two-, six-, and 12-minute walking tests in respiratory disease. Br Med J (Clin Res Ed) 1982;284 (May 6329)1607–8 Epub 1982/05/29.
[18] Parker M, Palmer C. A new mobility score for predicting mortality after hip fracture. J Bone Joint Surg Br 1993;75(5):797–8.
[19] Gao Z, Lv Y, Zhou F, Ji H, Tian Y, Zhang Z, et al. Risk factors for implant failure after fixation of proximal femoral fractures with fracture of the lateral femoral wall. Injury 2018;49(2):315–22.
[20] Ma Z, Yao X, Chang S. The classification of intertrochanteric fractures based on the integrity of lateral femoral wall: letter to the editor, fracture morphology of AO/OTA 31-a trochanteric fractures: a 3D CT study with an emphasis on coronal fragments. Injury 2017;48(10):2367–8.
[21] Chang SM, Zhang YQ, Ma Z, Li Q, Dargel J, Eysel P. Fracture reduction with positive medial cortical support: a key element in stability reconstruction for the unstable pertrochanteric hip fractures. Arch Orthop Trauma Surg 2015;135 (June 6)811–8 Epub 2015/04/05.
[22] Rodriguez A, Laio A. Machine learning. Clustering by fast search and find of density peaks. Science 2014;344(6191):1492–6.
[23] Hoffmann S, Paetzold R, Stephan D, Püschel K, Buehren V, Augat P. Biomechanical evaluation of interlocking lag screw design in intramedullary nailing of unstable pertrochanteric fractures. J Orthop Trauma 2013;27(9):483–90.
[24] Pradeep A, KiranKumar A, Dheenadhayalan J, Rajasekaran S. Intraoperative lateral wall fractures during Dynamic Hip Screw fixation for intertrochanteric fractures-Incidence, causative factors and clinical outcome. Injury 2018;49 (2):334–8.
[25] Bartoska R, Baca V, Kachlik D, Marvan J, Dzupa V. The correlation between muscles insertions and topography of break lines in pertrochanteric fractures: a comprehensive anatomical approach of complex proximal femur injuries. Surg Radiol Anat 2013;35(December 10)957–62 Epub 2013/04/30.